Chapter 4
Liquid Interface Self-Assembly with Colloidal Quantum Wells

Abstract In this chapter, we discuss our methodologies for the self-assembly of colloidal nanoplatelets (NPLs) at the liquid interface. We also review other recent studies on orientation-controlled platelet assembly on liquid interfaces. We compare the results of the reported studies and discuss the parameters that affect the NPL orientation at the liquid interface.

Keywords Liquid interface · Orientation control · Stacking · Planar waveguides

We use liquid interface self-assembly for deposition of highly homogeneous NPL thin films while achieving uniform control over NPL orientation and film thickness. Using conventional thin film deposition methods for NPLs such as spin-coating or drop-casting, it is possible to obtain NPL thin films with mixed orientation [1–4]. Furthermore, precise thickness control at the monolayer scale with these methods remains to be a challenge. Even though anti-solvent addition is shown to create intentional NPL stacking [5, 6], such films also suffer from large-scale uniformity.

In Sect. 4.1, we describe our methodology for the deposition of densely packed thin films of CdSe core NPLs as a single self-assembled monolayer with uniformly controlled (i.e. all face-down or all edge-up) orientation across the film [7]. We discuss in Sect. 4.2 the demonstration and characterization of the multilayered deposition of all-face-down self-assembled CdSe/CdZnS core/shell NPL films where control in the film thickness is achieved at monolayer precision. With these techniques, it has been possible to create highly homogeneous NPL films deposited across areas as large as several tens of cm^2. The area to be deposited can be in principle arbitrarily large and is only limited by the size of the container in which the self-assembly deposition is carried out.

O. Erdem and H. V. Demir, *Oriented Self-Assembly of Colloidal Semiconductor Nanoplatelets on Liquid Interfaces*, Nanoscience and Nanotechnology,
https://doi.org/10.1007/978-981-19-7052-8_4

4.1 Controlling the Orientation of Nanoplatelets on Liquid Interface

Orientation-controlled self-assembly of colloidal NPLs has two main advantages. The first one is that uniformly oriented NPL films enable studying the anisotropy in the NPLs by ensuring that the anisotropic effects are not evened out by dipoles of randomly oriented mixtures of NPLs. The second is that, with such oriented films, these direction-dependent properties can be exploited in optoelectronic applications.

Being able to control the NPL orientation in the solid film is a powerful tool for utilization of the NPLs in optoelectronic applications because, depending on the application of interest, one NPL orientation can be preferred over the other. For instance, due to the in-plane orientation of the band-edge dipoles of core NPLs [8], face-down NPL orientation is expected to increase the outcoupling efficiency in the NPL-LEDs. While the theoretical outcoupling efficiency of LEDs with isotropically emitting, spherical QDs is 20%, it could be as high as 40% with nanorods or NPLs with their emission dipoles oriented parallel to the substrate [9]. Similarly, face-down orientation would be the desired configuration in applications where NPLs are to be used as emitters, due to the observed FRET-assisted charge trapping in colloidal NPL stacks, which is detrimental to photoluminescence (PL) efficiency [8, 10, 11]. However, our work has shown, as will be discussed in Chap. 5, that a self-assembled monolayer of CdSe NPLs can act as a more efficient exciton sink layer when the ensemble adopts the stacked configuration rather than the face-down one [7]. A more recent study has demonstrated that the regularly stacked NPL ensembles with μm-long stacks can display higher conductivity as an n-channel of a thin-film transistor than randomly oriented NPL films with face-down NPLs and short and irregular stacks. Furthermore, for the stacked ensemble, conductivity of the film increases with the length of the stacks [12]. These examples show that the NPL orientation that is beneficial to the application can differ.

One of the earlier accounts of liquid interface self-assembly of organic-capped, platelet-shaped nanoparticles with uniformly dictated orientation is reported in 2011 [13]. Herein, the authors used ethylene glycol (EG) and its derivatives (di-, tri-, and tetraethylene glycol) as a subphase to deposit rhombic GdF_3 nanoplates with controlled orientation. They reported that the tendency of the nanoplates to form stacks increases with the polarity of the subphase. Therefore, the most polar subphase among this set, EG, led to lamellar nanoplate stacking, while the least polar of them, i.e. tetraethylene glycol, yielded face-down ("columnar") assemblies [13]. Mono- and multilayers of lamellar stacks and face-down assemblies of these nanoplates can be seen in Fig. 4.1a, b.

Using a similar approach, Gao et al. demonstrated orientation-controlled self-assembly of 5.5 ML CdSe core NPLs. In this work, they used mixtures of diethylene glycol (DEG) and oleic acid to tune the interfacial energy between the NPL

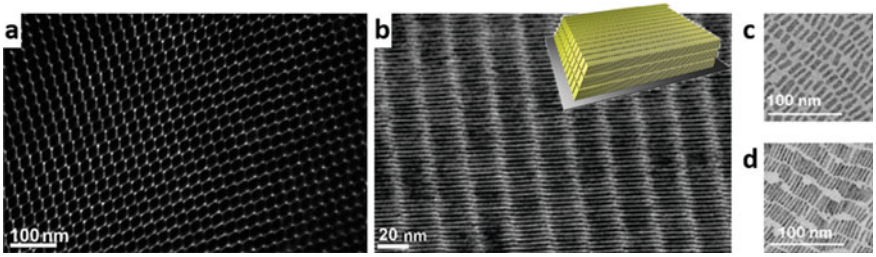

Fig. 4.1 **a** Multilayers of GdF_3 rhombic platelets with **a** face-down and **b** lamellar orientations. Inset in **b** depicts the tilting of the lamellar multilayers with respect to the substrate. Reprinted with permission from [13]. TEM imaging of **c** face-down and **d** edge-up assemblies of 5.5 ML CdSe core NPLs. Reprinted with permission from [8]. Copyright 2013, 2017 American Chemical Society

ligands and liquid surface, thereby to adjust the NPL orientation. Higher concentration (4.2 mM) of oleic acid in DEG resulted in the all-face-down orientation of the NPLs (Fig. 4.1c), while with a much lesser concentration of oleic acid (0.42 mM), the resulting NPL film was fully stacked (edge-up) (Fig. 4.1d). The sizes of the continuously deposited domains of the NPL film were as large as tens of μm. The k-space spectroscopy of these thin films revealed that the emission dipole of the core NPLs studied is almost completely confined within the plane of the NPLs, with no particular preference in the two in-plane directions [8].

In our 2019 work, we aimed to create a single self-assembled monolayer rather than multiple monolayers, all the while having high surface coverage on large scale. Our goal in creating such NPL films, as we explain in detail in Chap. 5, is to be able to study orientation-dependent interaction of self-assembled NPLs with colloidal quantum dots (QD) on an ensemble scale. The 4.5 ML CdSe core NPLs we used in this study were synthesized using a previously reported recipe [14] with slight modifications. The synthesized NPLs are square-shaped with an average side length of 14.4 nm [7].

The process of the liquid interfacial self-assembly that we developed and used with these NPLs is illustrated in Fig. 4.2a. Silicon-based substrates of 1×1 cm^2 size are initially submerged into the subphase, which is contained in a Teflon vessel. We drop solution of NPLs dissolved in hexane onto the liquid interface, close to the center of the surface. The hexane solution spreads across the interface while evaporating. After the evaporation is complete, a thin membrane of NPLs is formed on the liquid–air interface. To deposit this thin membrane onto the substrates, we drain the subphase fluid with the help of a needle (Fig. 4.2b), which penetrates the side wall of the teflon well, close to the bottom of it. This way, we ensure that the self-assembled membrane on the surface is not distorted until it is deposited onto the substrate. Even after the subphase is drained, some of it gets trapped in between the NPL membrane and the substrates in the form of droplets or a single, bigger dome across the substrate. This excess subphase is evaporated to complete the deposition. For ACN, waiting a few minutes under atmosphere suffices for complete evaporation

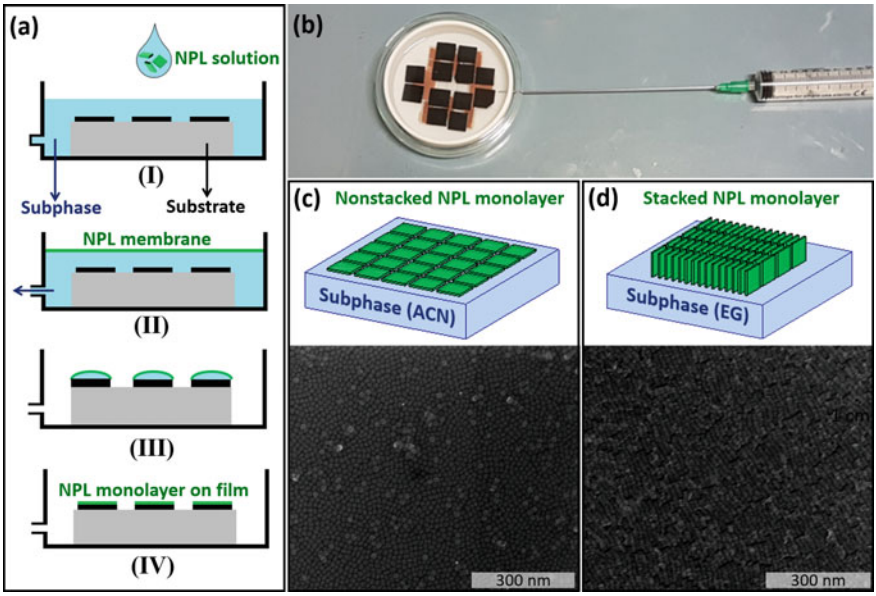

Fig. 4.2 Schematic process of the orientation-controlled liquid interfacial self-assembly of colloidal CdSe NPLs. (I) After the blank substrates are placed inside the subphase, the NPL solution is poured onto the surface of the subphase. (II) The hexane solution of NPLs spreads across the interface and is allowed to dry. (III) Subphase is extracted through a drain near the bottom of the well. (IV) Remaining droplets of subphase on the substrates are let dry. **b** Top view of the self-assembly setup. Diameter of the Teflon beaker is 64 mm. **c** Schematic representation of an NPL monolayer on the subphase of acetonitrile (ACN), along with the scanning electron microscopy image of the monolayer after the transfer to the substrate. **d** Schematic representation and the SEM image when the subphase chosen is ethylene glycol (EG). Adapted with permission from [7]. Copyright 2019 American Chemical Society

while for excess EG, it is often necessary to keep the samples under vacuum for a few days.

The amount of NPL solution to be dropped onto the subphase has been determined based on the concentration of the solution, which has been estimated as 2.1×10^{-7} M using the work of Yeltik et al. [15]. To approximately fill the entire liquid interface of 64 mm in diameter, we dropped about 60 μL of the NPL solution having this concentration. For the stacked NPL assembly, to account for the expected tighter packing due to the NPLs standing upright on their peripheral edge rather than lying flat on their lateral surfaces, the concentration was doubled (4.2×10^{-7} M) while still dropping 60 μL of solution. It should be noted that the resulting membranes do not cover the entire surface of the interface, but rather most of it, which is sufficient to create close-packed, continuous domains of several mm^2 in film, as shown and discussed below.

Scanning electron microscopy (SEM) images of face-down and edge-up assemblies are presented in Fig. 4.2c and Fig. 4.2d, respectively. The NPLs assembled on

ACN are seen to have a face-down configuration. Furthermore, apart from minor irregularities, they are deposited as a uniform, tightly packed single monolayer onto the substrate. The NPLs self-assembled on EG also display nicely ordered, edge-up stacking as a single monolayer with no apparent irregularity or multilayer formation. The NPL stacks monitored in Fig. 4.2d are aligned with each other and elongated in the same direction. This alignment is observed to be limited to at most several μms, typically bounded with other grains of NPL stacks aligned in another direction. This local alignment of NPL chains suggests that the NPL stacks have a tendency to align side by side, similar to the alignment of μm-long needles in the work of Abécassis et al. [6]. However, since this stack alignment is taking place locally and simultaneously everywhere across the liquid interface, the directional alignment is limited to the individual grains.

The SEM images with lower magnification in Fig. 4.3 confirm that the domains of tightly packed NPLs are as large as several mm^2. Occasionally, cracks in the membrane, such as those in Fig. 4.3d can occur, during the transfer of the membrane onto the substrate. In order to reduce the risk of this kind of crack formation, and

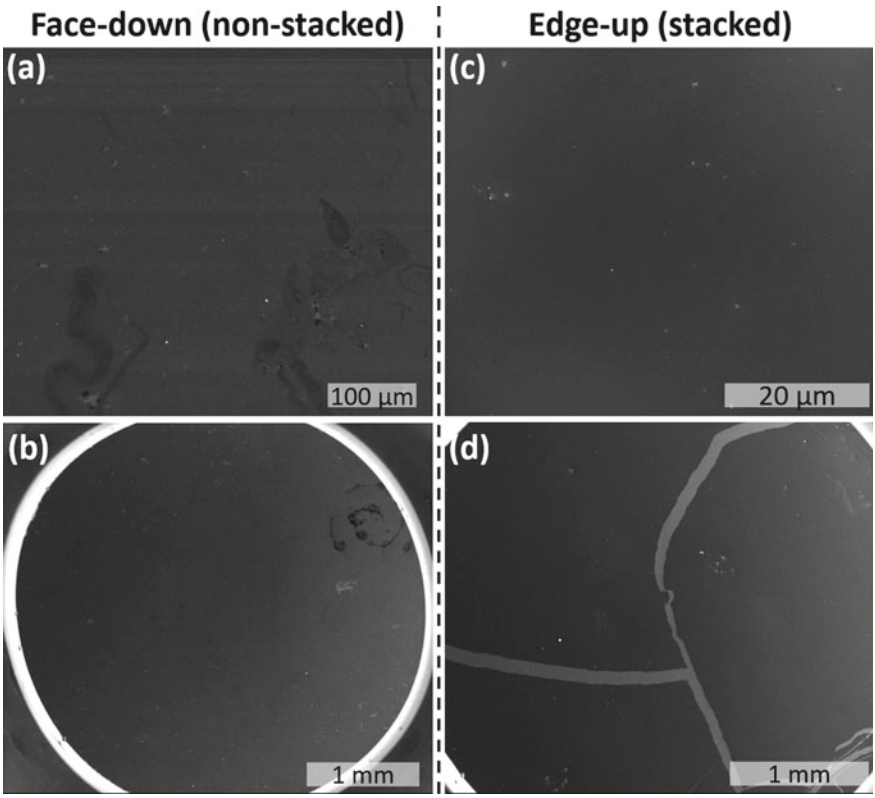

Fig. 4.3 SEM images of **a**, **b** face-down and **c**, **d** edge-up NPL ensembles at lower magnifications. Adapted with permission from [7]. Copyright 2019 American Chemical Society

thereby to increase the size of the domains, we have incorporated a silicone oil (Sylgard 184) diluted with hexane (~1.5 mg/mL) in the self-assembly process. The presence of silicone oil enables compression of the membrane on the liquid interface. As a result, the previously separated, mm-sized domains are brought together and deposited as a single, close-packed membrane onto the substrate. To demonstrate that this could increase the domain size, we have performed the self-assembled deposition of NPLs onto a 2-inch silicon wafer with thermally grown thermal oxide on top. The silicone oil solution is dropped onto the edge of the liquid surface, to a small blank area, as shown in Fig. 4.4a. The photographs of the 2-inch wafers deposited with face-down and edge-up NPL monolayers under UV light are shown in Fig. 4.4b and Fig. 4.4c, respectively.

In these photos, a significant difference between the edge-up film can be noticed, when viewed from the top (Fig. 4.4b, right) and when viewed from 45° (Fig. 4.4c, right). While having the characteristic green emission of 4.5 ML CdSe core NPLs

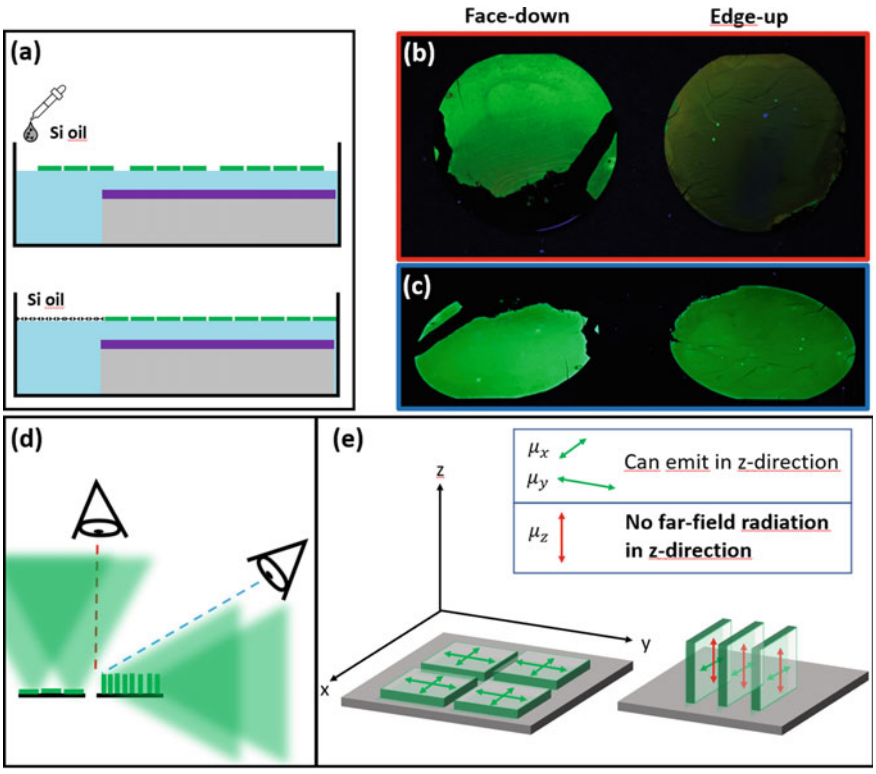

Fig. 4.4 **a** Compression of NPL membranes with silicone oil. **b**, **c** Photographs of face-down and edge-up NPL monolayers deposited on a 2-inch wafer of thermally grown silicon oxide on silicon, illuminated with UV light. Photographs are taken from the top in **b** and at approximately 45° in **c**. **d** Camera angles in the photos along with the largely out-of-plane emission schematically illustrated. **b**, **c** Adapted with permission from [7]. Copyright 2019 American Chemical Society

when viewed at 45°, the film of edge-up NPLs appears to have a weaker emission from the top with greenish yellow color. This initially unanticipated phenomenon could be explained by two different effects. Firstly, if there are defective NPL subspecies, the energy transfer-assisted charge trapping is greatly enhanced in stacked NPL ensembles, which causes a reduction in PL efficiency [10]. Secondly, due to the emission dipoles being confined within the NPL plane, the NPL far-field emission will be majorly directed out of the NPL plane. As a result, while both components of the emission dipoles of face-down NPLs will generate far-field emission in the vertical direction away from the substrate, for the edge-up NPLs, only the dipoles in a single direction will contribute to the out-of-substrate far-field emission (Fig. 4.4e). Therefore, the green emission that can be observed from directly above the stacked NPL ensembles is reduced to a great extent, while it can still be seen at lower angles as both dipole components in stacked NPLs still contribute to the far-field radiation in the two other directions (see Fig. 4.4d, e). The yellowish tone that is instead perceived from the top could be a combination of weakened green emission in the z-direction and the spectrally broad trap state emission of NPLs centered in red [16, 17].

The orientation-controlled NPL monolayers that are self-assembled onto 1×1 cm^2 silicon-based substrates were used as acceptors in a nonradiative energy transfer working model system. The results of this distance- and orientation-dependent energy transfer study will be discussed in Chap. 5.

4.2 Multilayered Deposition of Self-Assembled NPLs

The work on liquid interface self-assembly that has been discussed so far focused on the deposition of NPLs at one step by transferring a single NPL membrane to the substrate. The thickness of this membrane could be a single monolayer or multiple monolayers. However, variation in film thickness is commonly observed with NC films deposited by one-step liquid interfacial assembly [13, 18, 19]. To achieve uniformity in thickness and to be able to deposit NPL films having any desired thickness, we use sequential deposition of self-assembled NPL monolayers using liquid interface self-assembly. Our work and results that we present in this section are adapted with permission from [20]. Copyright 2020 American Chemical Society.

To create multilayered, optically active NPL waveguides, we deposit face-down layers of CdSe/$Cd_{0.25}Zn_{0.75}S$ core/shell NPLs. These NPLs, which were synthesized using our previously reported recipe, have cores of 4.5 ML thickness, which were shelled using a hot-injection technique [21]. The thickness of their inorganic part is ~4.1 nm as determined from TEM imaging [20]. With these NPLs, DEG was chosen as the subphase in the self-assembly process as it yielded the most homogeneous all-face-down films with excellent uniformity.

To deposit multilayered colloidal NPLs sequentially on the same substrate, we introduce some modifications to our recipe we described in the previous section. To shorten the duration of evaporation in between the successive deposition cycles, we have introduced a tilt angle of around 10° for the substrates that are immersed in the

subphase. Additionally, we have pre-treated our silicon and fused silica substrates with the vapor of 1H, 1H, 2H, 2H-perfluorodecyltriethoxysilane under nitrogen environment at 200 °C. This treatment renders the surface of our substrates highly hydrophobic [22]. In addition to water, these treated surfaces also repel other polar liquids that we use as subphase. Owing to the combination of this substrate treatment and tilting, the subphase of DEG is easily repelled away by the substrates as it is drained out of the beaker. This leaves little or no noticeable residual DEG on the substrates, which greatly shortens the evaporation time under vacuum from a few days to a few hours.

The modified self-assembly procedure is schematically described in Fig. 4.5a. Blank or previously deposited substrates are inserted into DEG subphase. Twenty-five microliters of NPL solution in hexane (5.5×10^{-7} M) are then dropped onto the subphase and quickly spreads across the subphase interface. One drop (~10 μL) of silicone oil solution (silicone elastomer, Sylgard 184, ~1.5 mg/mL in hexane) is used to compress the NPL membrane toward the substrate side. After complete evaporation of hexane, DEG is drained out with a peristaltic pump at the rate of 50 μL/min. This rate corresponds to ~260 nm descent of liquid per second in the Teflon dish used as the container for the self-assembly deposition [20].

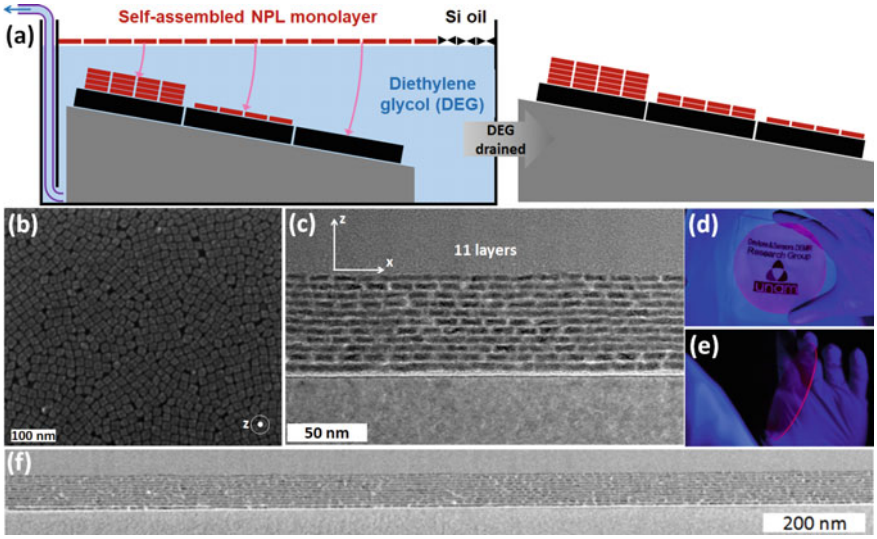

Fig. 4.5 **a** Schematic description for the multilayered self-assembly deposition of $CdSe/Cd_{0.25}Zn_{0.75}S$ core/shell NPLs. At the end of a deposition cycle, all substrates are deposited with one additional NPL monolayer. **b** SEM image of a single self-assembled monolayer of $CdSe/Cd_{0.25}Zn_{0.75}S$ NPLs. **c** Cross-sectional TEM image of 11-NPL monolayers sequentially deposited onto silicon. Photograph of a UV-illuminated 4-inch fused silica wafer deposited with one monolayer of NPLs **d** from the top and **e** from the side. **f** TEM image of the cross-section in **c** at a lower magnification. Adapted with permission from [20]. Copyright 2020 American Chemical Society

At the end of this procedure, one full monolayer of NPLs is deposited onto the substrates inside the Teflon crucible. The SEM image in Fig. 4.5b confirms that this NPL monolayer is composed entirely of tightly packed, face-down NPLs with excellent uniformity and no visible aggregation or multilayers. Figure 4.5c displays the cross-sectional TEM image of a silicon substrate deposited with this procedure 11 times, resulting in an 11-layered NPL film. All the NPL monolayers in this micrograph are distinctly visible, separated by their organic ligands. The TEM image of the same cross-sectional sample across a ~2 μm range is given in Fig. 4.5f. Similar to Fig. 4.5c, no irregularity is observed across the NPL monolayers.

To demonstrate that this self-assembly technique is adequate for the deposition of arbitrarily large surfaces, we have deposited a fused silica wafer with a 4-inch diameter with one self-assembled NPL monolayer. The photograph of the deposited wafer in Fig. 4.5d shows that the entire wafer is deposited with NPLs with uniform emission throughout the wafer.

The tight packing of the self-assembled NPLs is secured by the presence of silicone oil on the liquid interface. Once dropped in sufficient amount, silicone oil ensures that the membrane will be forced to stay on the substrate during the transfer instead of being swept away together with the DEG. To better observe and understand the role of the silicone oil in this self-assembly method, we have deposited films of single monolayer NPLs with and without the silicone oil. The SEM images in Fig. 4.6a, b show that without the assistance of silicone oil, a significant portion of the substrate surface remains uncoated. In contrast, films self-assembled with silicone oil (Fig. 4.6c, d) display near-unity surface coverage with excellent uniformity and a negligible amount of gaps within the film. The compression effect of the silicon oil could also be observed during deposition on the liquid interface. After the addition of silicone oil, the red-emitting NPL membrane is noticeably compressed (Fig. 4.6e, f) [20]. The amount of compression depends on the initial NPL concentration and amount.

To further elaborate on the homogeneity of the NPL multilayers, we have used characterization tools such as ellipsometry, atomic force microscopy (AFM), and micro-PL spectroscopy on the multilayered NPL films. The film thicknesses measured via ellipsometry are plotted in Fig. 4.7a, which confirms the expected linear trend between the film thickness and the number of NPL monolayers. The slope of the linear fitting is 7.0 nm/layer, indicating that each deposited NPL layer adds up to 7.0 nm to film thickness. Since the thickness of the core/shell structure is 4.1 nm, this means that the average thickness of the ligand brush in between two consecutive NPL monolayers is 2.9 nm. This thickness, which is slightly less than twice the length of the oleic acid molecule (1.8 nm), suggests a partial interdigitation between the ligand brushes. This interdigitation might help the NPL monolayers stick together via van der Waals interaction, adding to the robustness of the film. As opposed to layer-by-layer NC deposition via dip coating, where deposition of an oppositely charged linker molecule between each monolayer is required [23–25], the self-assembled NPL monolayers could be deposited directly one on top of another while maintaining large-area uniformity and precision in film thickness. The uniformity in micro-scale is further corroborated with AFM imaging on multilayered NPL

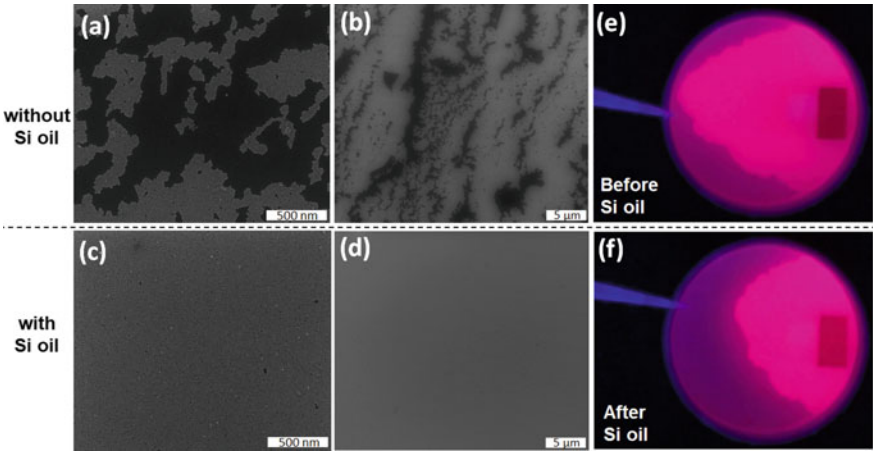

Fig. 4.6 SEM images of a single self-assembled NPL monolayer **a**, **b** without and **c**, **d** with the silicone oil. The dark areas on the images show voids, while the gray areas are filled. Scale bars are 500 nm in **a**, **c** and 5 μm in **b**, **d**. Photograph of an NPL membrane illuminated with UV excitation **e** before and **f** after the silicone oil is added. Reprinted with permission from [20]. Copyright 2020 American Chemical Society

films across $2 \times 2\ \mu m^2$ regions. A plot of the root mean square (rms) roughness of multilayer surface versus the number of layers in Fig. 4.7c shows that the rms roughness is barely larger than 1 nm for the thickest NPL multilayers studied (15 layers ≡ 105 nm). This means that a film thicker than 100 nm could be deposited uniformly with about a 1% variation in thickness.

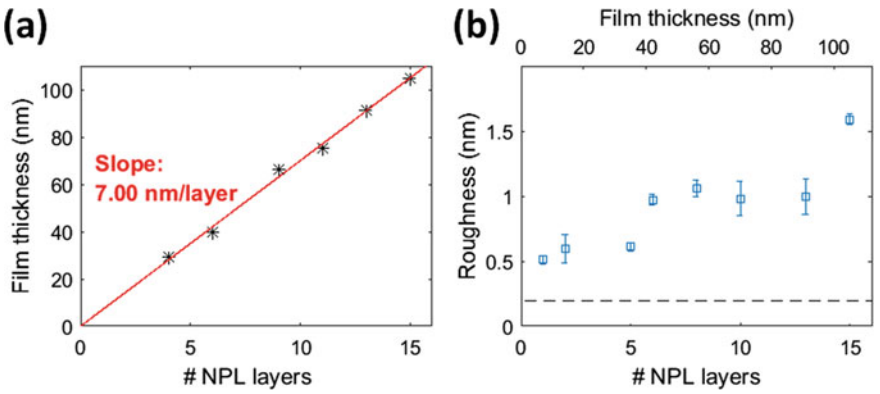

Fig. 4.7 **a** Ellipsometry measurements on multilayered NPL films with different numbers of layers ranging from 4 to 15. Slope of the film thickness as a function of the number of NPL layers is found to be 7.0 nm/layer. **b** Roughness measurements taken from the atomic force microscopy scans of NPL multilayers. Dashed line indicates the roughness of the blank substrate (~0.2 nm). Reprinted with permission from [20]. Copyright 2020 American Chemical Society

To test the homogeneity of our multilayered NPL films on macro-scales we have used ellipsometry and micro-PL spectroscopy. The PL mapping of a 14-layered NPL film, taken at four different spots of ~$100 \times 100\,\mu m^2$ size, is seen to be nearly identical (Fig. 4.8a, b). In addition, ellipsometry measurements at five different spots on a ten-layered sample revealed that the thicknesses at these different spots are virtually equal, ranging from a minimum of 68.6 nm to a maximum of 69.4 nm (Fig. 4.8c, d).

In summary, we have verified the homogeneity of the multilayered films constructed via liquid interface self-assembly using scanning electron and atomic force microscopies at the microscale, and ellipsometry and micro-PL spectroscopy at the device scale. The near perfection of the films at the single monolayer level extends into unprecedented homogeneity in film thickness of multilayers in the several tens of cm^2 scale. Though we did observe a few irregularities and gaps in some of the SEM images of self-assembled monolayers [20], the occurrence of these across the monolayer is extremely rare and does not have a noticeable effect in, for instance, the multilayered NPL arrays in Fig. 4.5f.

In Chap. 5, we will discuss the prospect of these NPL multilayers as optically active waveguides and gain media.

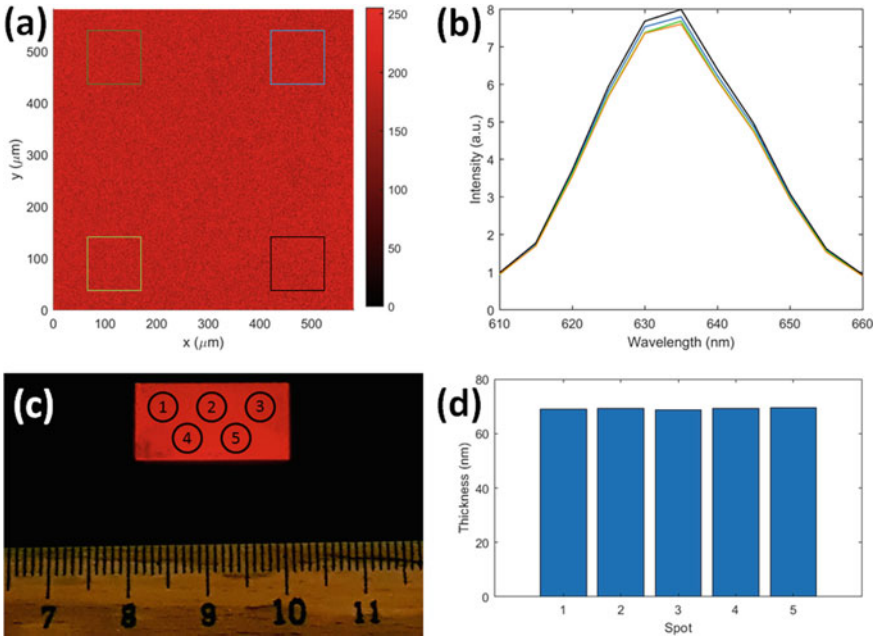

Fig. 4.8 **a** PL mapping of the 14-layered NPL film taken with a confocal microscope. **b** PL spectra collected at four different spots (marked with colored squares in panel **a** on the studied region). **c** Photograph of the 10-layered NPL film deposited onto a 2×1 cm^2 substrate of fused silica. **d** Results of the thickness measurement on the five spots of the film shown in **c** via ellipsometry. **a–c** Reprinted with permission from [20]. Copyright 2020 American Chemical Society

4.3 Other Approaches to Liquid Interface NPL Self-Assembly: Parameters that Affect NPL Orientation

The aforementioned studies on liquid interfacial NPL assembly in Sect. 4.1 have adopted the approach of controlling the NPL orientation by choosing the subphase to modify interactions between the liquid interface and NPL ligands. In their study on the self-assembly of platelet-shaped GdF_3 nanoparticles, Paik et al. concluded that the preferential alignment of their oleate-capped platelets is dictated by the subphase, specifically, its polarity [13]. A similar reasoning has been used for the in-film phase adapted by the ensembles of octadecylphosphonic acid capped CdSe/CdS dot-in-rod NCs, where it has been proposed that the interaction energy between the NC ligands and the subphase depends on the surface tension of the subphase used [26]. The work by Erdem et al. also demonstrated that the use of a highly polar subphase leads to edge-up NPL ensembles, while a subphase with lesser polarity results in face-down orientation [7]. These results suggest that the hydrophobic alkyl chains bound to the NPL surfaces display stronger repulsion against more polar subphases and are forced to attach to each other to minimize their contact with the surface of the subphase.

A more recent report followed a different approach for liquid air interface self-assembly. Herein, the authors deposited orientation-controlled monolayers of 4.5 ML NPLs while using the same subphase, acetonitrile (ACN), in both cases, but dictated the NPL orientation by controlling the evaporation rate of the NPL solution after dropping it onto the ACN interface. In this approach, slowing down the evaporation rate in the system gives the NPLs in the ensemble sufficient time to adopt the thermodynamically favored edge-up orientation [27]. Their results show that solvent evaporation rate is among the factors that determine the orientation of the NPLs in liquid interface self-assembly.

In Table 4.1, we provide a list of the recent studies on liquid interface self-assembled NPLs, mostly on CdSe-based NPLs. Even though GdF_3 belongs to an entirely different class of materials than our Cd-based semiconductor NCs, we also choose to include the results of [13] in this comparison as this report influenced the follow-up work with its methodology and the choice of subphases. Furthermore, similar to the self-assembled CdSe-based NPLs, the GdF_3 platelets are also capped with organic ligands; therefore the results of this work are highly relevant to the liquid interface assembly of CdSe-based NPLs, particularly in terms of ligand-subphase interactions.

In general, the reports in which face-down NPL ensembles are obtained use subphases having weaker polarity such as ACN or dimethylformamide, with the exception of Ref. [27], where slow-evaporation induced stacking on ACN is demonstrated. On the other end, using subphases as polar as EG appears to induce stack formation in NPLs, based on the results of Refs. [7] and [13]. It is interesting to note that, though having a high polarity, DEG resulted in complete face-down orientation (Fig. 4.5b) in the self-assembly of CdSe/CdZnS core/shell NPLs [20]. Even with EG, which has even stronger polarity than DEG, only partial stacking could be initiated

Table 4.1 Comparison of recently published reports on liquid interface self-assembly of colloidal NPLs. Subphase abbreviations: EG, ethylene glycol; DEG, diethylene glycol; 3EG, triethylene glycol, 4EG, tetraethylene glycol; ACN, acetonitrile; DMF, dimethylformamide

Report	NPLs	Solvent	Ligand	Subphase	Orientation	Notes
Ref. [13] (2011)	GdF_3	Hexane	Oleic acid (OA)	EG	Edge-up*	*Lamellar stacking. NPLs are tilted w.r.t. substrate
				DEG	Mixed	
				3EG	Face-down	
				4EG	Face-down	
Ref. [8] (2017)	5.5 ML CdSe	Hexane	Oleic acid	OA in DEG (4.2 mM)	Face-down	
				OA in DEG (0.42 mM)	Edge-up	
Ref. [7] (2019)	4.5 ML CdSe	Hexane	Oleic acid	ACN	Face-down	
				EG	Edge-up	
Ref. [27] (2020)	4.5 ML CdSe	Hexane	Myristic acid	ACN	Face-down*	*Controlled by the rate of solvent evaporation
				ACN	Edge-up*	
Ref. [20] (2020)	CdSe/CdZnS core/shell	Hexane	Oleic acid, oleylamine	DEG	Face-down	
Ref. [19] (2021)	CdSe/CdZnS core/shell	Chloroform	Oleylamine	Oleylamine in DMF (5 mM)	Face-down	
	CdSeS/CdZnS core/shell					

in the same batch as seen in Fig. 4.9. It can be observed here that the fraction of edge-up-oriented NPLs is rather limited and the majority of the NPLs remain face-down. The stark contrast between EG-interface self-assembly of core CdSe NPLs (Fig. 4.2c) and that of CdSe/CdZnS core/shell NPLs (Fig. 4.9) could be related to the thickness of the particles. While 4.5 ML CdSe cores are thin (having a thickness of 1.2 nm), the shelled CdSe/CdZnS NPLs used in Ref. [20] are much thicker (>4 nm). It is possible that these more massive NPLs require stronger repulsion between the subphase and their ligands and/or much slower solvent evaporation in order to settle down into the edge-up configuration.

It should be noted that there are possibly quite a few parameters other than the subphase and the evaporation rate that affect the NPL orientation, such as the concentration of NPLs and ligands, lateral area of the NPLs, and ambient temperature. For a more thorough understanding of the phenomenon of self-assembly on liquid interfaces, all of these additional parameters must be carefully taken into account.

For further reading on NPL assembly, we refer to [28].

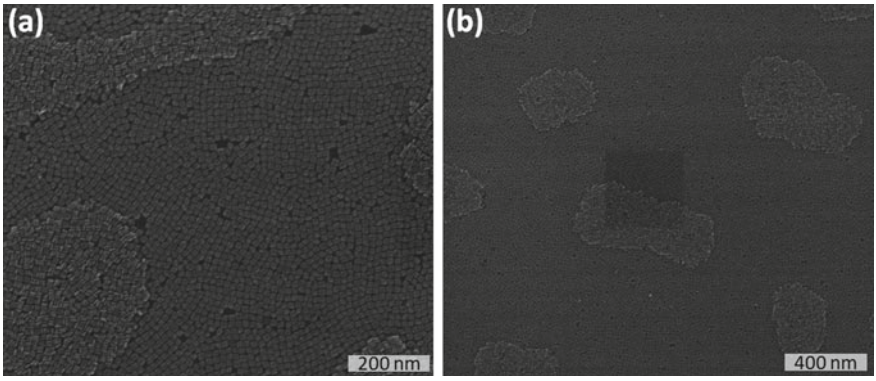

Fig. 4.9 SEM imaging of liquid interface self-assembled CdSe/CdZnS core/shell NPLs on ethylene glycol at **a** higher and **b** lower magnification. Partial stacking formation manifests itself as islands that are composed of NPLs having both face-down and edge-up orientations (2018 Demir Group)

References

1. She C, Fedin I, Dolzhnikov DS et al (2015) Red, yellow, green, and blue amplified spontaneous emission and lasing using colloidal CdSe nanoplatelets. ACS Nano 9:9475–9485
2. Guzelturk B, Olutas M, Delikanli S et al (2015) Nonradiative energy transfer in colloidal CdSe nanoplatelet films. Nanoscale 7:2545–2551
3. Feng F, Nguyen LT, Nasilowski M et al (2018) Probing the fluorescence dipoles of single cubic CdSe/CdS nanoplatelets with vertical or horizontal orientations. ACS Photon 5:1994–1999
4. Yang G, Kazes M, Oron D (2018) Chiral 2D colloidal semiconductor quantum wells. Adv Funct Mater 28:1802012
5. Tessier MD, Mahler B, Nadal B et al (2013) Spectroscopy of colloidal semiconductor core/shell nanoplatelets with high quantum yield. Nano Lett 13:3321–3328
6. Abécassis B, Tessier MD, Davidson P, Dubertret B (2014) Self-assembly of CdSe nanoplatelets into giant micrometer-scale needles emitting polarized light. Nano Lett 14:710–715
7. Erdem O, Gungor K, Guzelturk B et al (2019) Orientation-controlled nonradiative energy transfer to colloidal nanoplatelets: engineering dipole orientation factor. Nano Lett 19:4297–4305
8. Gao Y, Weidman MC, Tisdale WA (2017) CdSe nanoplatelet films with controlled orientation of their transition dipole moment. Nano Lett 17:3837–3843
9. Kim WD, Kim D, Yoon DE et al (2019) Pushing the efficiency envelope for semiconductor nanocrystal-based electroluminescence devices using anisotropic nanocrystals. Chem Mater 31:3066–3082
10. Guzelturk B, Erdem O, Olutas M et al (2014) Stacking in colloidal nanoplatelets: tuning excitonic properties. ACS Nano 8:12524–12533
11. Rowland CE, Fedin I, Zhang H et al (2015) Picosecond energy transfer and multiexciton transfer outpaces Auger recombination in binary CdSe nanoplatelet solids. Nat Mater 14:484–489
12. Jana S, Martins R, Fortunato E (2022) Stacking-dependent electrical transport in a colloidal CdSe nanoplatelet thin-film transistor. Nano Lett 22:2780–2785
13. Paik T, Ko DK, Gordon TR et al (2011) Studies of liquid crystalline self-assembly of GdF3 nanoplates by in-plane, out-of-plane SAXS. ACS Nano 5:8322–8330
14. Tessier MD, Spinicelli P, Dupont D et al (2014) Efficient exciton concentrators built from colloidal core/crown CdSe/CdS semiconductor nanoplatelets. Nano Lett 14:207–213

15. Yeltik A, Delikanli S, Olutas M et al (2015) Experimental determination of the absorption cross-section and molar extinction coefficient of colloidal CdSe nanoplatelets. J Phys Chem C 119:26768–26775
16. Erdem O, Olutas M, Guzelturk B et al (2016) Temperature-dependent emission kinetics of colloidal semiconductor nanoplatelets strongly modified by stacking. J Phys Chem Lett 7:548–554
17. Hinterding SOM, Salzmann BBV, Vonk SJW et al (2021) Single trap states in single CdSe nanoplatelets. ACS Nano 15:7216–7225
18. Dong A, Chen J, Vora PM et al (2010) Binary nanocrystal superlattice membranes self-assembled at the liquid-air interface. Nature 466:474–477
19. Samadi Khoshkhoo M, Prudnikau A, Chashmejahanbin MR et al (2021) Multicolor patterning of 2D semiconductor nanoplatelets. ACS Nano 15:17623–17634
20. Erdem O, Foroutan S, Gheshlaghi N et al (2020) Thickness-tunable self-assembled colloidal nanoplatelet films enable ultrathin optical gain media. Nano Lett 20:6459–6465
21. Altintas Y, Gungor K, Gao Y et al (2019) Giant alloyed hot injection shells enable ultralow optical gain threshold in colloidal quantum wells. ACS Nano 13:10662–10670
22. Beck M, Graczyk M, Maximov I et al (2002) Improving stamps for 10 nm level wafer scale nanoimprint lithography. Microelectron Eng 61–62:441–448
23. Ozel T, Nizamoglu S, Sefunc MA et al (2011) Anisotropic emission from multilayered plasmon resonator nanocomposites of isotropic semiconductor quantum dots. ACS Nano 5:1328–1334
24. Suarez I, Munoz R, Chirvony V et al (2017) Multilayers of CdSe/CdS/ZnCdS core/wings/shell nanoplatelets integrated in a polymer waveguide. IEEE J Sel Top Quantum Electron 23:1–8
25. Roither J, Pichler S, Kovalenko MV et al (2006) Two- and one-dimensional light propagations and gain in layer-by-layer-deposited colloidal nanocrystal waveguides. Appl Phys Lett 89:111120
26. Diroll BT, Greybush NJ, Kagan CR, Murray CB (2015) Smectic nanorod superlattices assembled on liquid subphases: structure, orientation, defects, and optical polarization. Chem Mater 27:2998–3008
27. Momper R, Zhang H, Chen S et al (2020) Kinetic control over self-assembly of semiconductor nanoplatelets. Nano Lett 20:4102–4110
28. Guillemeney L, Lermusiaux L, Landaburu G et al (2022) Curvature and self-assembly of semi-conducting nanoplatelets. Commun Chem 5:1–11